https://doi.org/10.5194/egusphere-2026-1853
Preprint. Discussion started: 5 June 2026

Evolution of firework-related barium aerosols: insights from single-particle analysis and mass concentration monitoring

Xiufeng Lian[1, 2], Chenglei Pei[3], Wei Sun[4], Chen Lv[5], Kunlun Huang[3], Lei Lei[3], Bo Huang[2], Chunlei Cheng[1], Guohua Zhang[4], Xinhui Bi[4], Zhen Zhou[1], Mei Li[1,*]

1 College of Environment and Climate, Institute of Mass Spectrometry and Atmospheric Environment, Guangdong Provincial Engineering Research Center for On-line Source Apportionment System of Air Pollution, Jinan University, Guangzhou 510632, China

2 Guangzhou Hexin Instrument Co., Ltd., Guangzhou 510530, China

3 Guangzhou Sub-branch of Guangdong Ecological and Environmental Monitoring Center, Guangzhou 510006, China

4 State Key Laboratory of Organic Geochemistry and Guangdong Provincial Key Laboratory of Environmental Protection and Resources Utilization, Guangzhou Institute of Geochemistry, Chinese Academy of Sciences, Guangzhou 510640, China

5 College of Ecology and Environment, Zhengzhou University, Zhengzhou 450001, China

*Correspondence to: Mei Li (limei@jnu.edu.cn)

Abstract. Fireworks are a well-known source of barium (Ba) in the atmosphere, yet their aging processes remain poorly understood. Using single-particle aerosol mass spectrometry (SPAMS) in Guangzhou, China, we show that firework events elevated atmospheric Ba concentrations by 1–3 orders of magnitude above background levels. The highest concentrations occurred in restricted zones rather than the more densely populated urban core, demonstrating the effectiveness of local restriction policies. Critically, we identified two distinct mixing states along the aging continuum, chloride-rich OClN particles (containing $BaCl_2$) and nitrate-dominated N particles (containing $Ba(NO_3)_2$). This chemical conversion co-occurred with physical coagulation involving Al/Mg-containing particles, which mixed preferentially with OClN over N. Observed lags of several hours between OClN and N peaks and between NO_2 and particulate NO_3^- point to nitrate formation as a key aging pathway. These findings elucidate the rapid aging mechanisms of firework-derived Ba particles and provide direct evidence that emission controls effectively mitigate firework pollution.

https://doi.org/10.5194/egusphere-2026-1853
Preprint. Discussion started: 5 June 2026

1 Introduction

Barium (Ba) is a potentially toxic element whose health effects depend strongly on its chemical form (Kaur and Parkash, 2022; Sharma and Thakur, 2025). In the atmosphere, Ba originates from both natural sources (e.g., mineral dust, volcanic emissions) and anthropogenic activities (Inomata et al., 2009). Among anthropogenic sources, fireworks represent a major episodic contributor during global celebrations such as New Year's Eve, Diwali, and the Chinese Spring Festival (Hu et al., 2015; Kong et al., 2015; Lee et al., 2023). During these events, fireworks can contribute up to 87% of ambient Ba, leading to concentrations several to thousands of times higher than background levels (Hu et al., 2015; Huang et al., 2024; Kulshrestha et al., 2004; Salma et al., 2023; Tanda et al.,2019; Wang et al.,2024). This pronounced transient signal makes Ba an effective tracer for firework-derived pollution (Wang et al., 2024), providing a unique opportunity to study the atmospheric processing of metal-containing aerosols.

Fireworks are complex pyrotechnic mixtures containing oxidizers (e.g., $KClO_3$, $KClO_4$, $Ba(NO_3)_2$), fuels (e.g., sulfur, charcoal, aluminum), and colorants that produce specific metal emissions (Webster, 1985). For green fireworks, Ba compounds such as $BaCl_2$, $Ba(NO_3)_2$, and $Ba(ClO_3)_2$ are commonly used as colorants, with $BaCl_2$ being the most widely employed due to its intense green emission and favorable combustion properties (Li et al., 2013; Wang et al., 2007). Upon ignition, these Ba salts are rapidly vaporized and subsequently condense to form primary particles, which are initially enriched in chlorine (e.g., $BaCl_2$) or, depending on the formulation, in nitrate or perchlorate (Wang et al., 2007).

Despite the well-documented surge in Ba concentrations during fireworks events, the chemical speciation of ambient Ba-containing particles remains poorly understood and debated (Li et al., 2013; Webster et al., 1985; Wang et al., 2007). While fresh firework emissions are typically chlorine-rich (e.g., $BaCl_2$), field observations often report aged particles enriched in sulfur rather than chlorine, suggesting atmospheric transformation during transport (Li et al., 2013; Wang et al., 2007). For firework-generated particles (e.g., potassium-containing), both sulfation and nitration have been observed during aging (Wang et al., 2024). However, whether analogous transformations occur for Ba-containing particles remains largely unexplored. In this study, we investigate the aging mechanisms of firework-generated Ba aerosols from a single-particle perspective, with a focus on nitrate-mediated pathways.

The environmental and health impacts of firework-derived Ba are fundamentally governed by its chemical speciation (Inomata et al., 2009). Soluble forms such as $BaCl_2$ and $Ba(NO_3)_2$ are highly bioavailable and pose acute toxicity risks upon inhalation (Kaur and Parkash, 2022), whereas insoluble species like $BaSO_4$ exhibit low chemical toxicity but contribute to long-range transport as fine suspended particles (Inomata et al., 2009; Sharma and Thakur, 2025). Given that atmospheric aging processes, including heterogeneous reactions, gas-to-particle conversion, and physical coagulation, can fundamentally alter the chemical speciation of aerosol particles (Zhang et al., 2015), understanding how these processes apply to Ba-containing particles is essential for predicting their environmental fate and health impacts. For metal-containing particles, aging can involve the uptake of acidic gases such as NO_2 and HNO_3, leading to the formation of nitrates on particle surfaces

https://doi.org/10.5194/egusphere-2026-1853
Preprint. Discussion started: 5 June 2026

(Liu et al., 2017; Peng et al., 2021).

To address these knowledge gaps, we conducted continuous online monitoring of aerosols in Guangzhou, China, over a one-month period spanning the Spring Festival, using single-particle aerosol mass spectrometers (SPAMS) and online heavy metal monitors. This approach allows us to obtain high temporal resolution data on the chemical composition and size distribution of Ba-containing particles at the single-particle level, as well as mass concentrations of Ba in $PM_{2.5}$. Leveraging these high-resolution measurements, we systematically investigate the variation characteristics of Ba aerosols in relation to fireworks events, elucidate the aging mechanisms of Ba-containing particles in the ambient atmosphere, and provide a preliminary assessment of their potential health implications based on mass concentration data. This study contributes to a more comprehensive understanding of the atmospheric fate of firework-derived metal aerosols and their associated health risks, with implications for air quality management and public health policy in regions where fireworks are traditionally used.

2 Field measurements

2.1 Sampling sites and period

This study was conducted in Guangzhou, China, from February 1st to 29th, 2024, covering the key periods of legal fireworks use during the Chinese New Year (February 9–10 and February 24). Fireworks management followed the tiered control policy of the Guangzhou Fireworks and Firecrackers Safety Management Regulation, which designates central urban districts as prohibited zones and peripheral districts as restricted zones where fireworks are permitted only during specified periods (Guangzhou Municipal People's Government, 2021).

Four monitoring sites were established across Guangzhou: Gongyuanqian (GYQ; 23.13° N, 113.25° E) in Yuexiu District, a prohibited zone in the central urban area; Panyu University City (PYDXC; 23.05° N, 113.39° E) and Nansha Puzhou (NSPZ; 22.77° N, 113.60° E) in restricted zones of Panyu and Nansha districts; and Conghua Liangkou (CHLK; 23.74° N, 113.78° E), a sparsely populated area serving as an urban background site.

2.2 Data analysis and presentation strategy

Hourly concentrations of trace metals, including Ba, were measured using an online ambient metal monitor (Xact 625i, Cooper Environmental) based on energy-dispersive X-ray fluorescence(Twohy et al., 2010). Water-soluble ions (nitrate, sulfate, ammonium, chloride) were quantified by an online ion chromatography system (Metrohm, 6080). Single-particle chemical composition in the 0.2–2.0 μm size range was characterized in real-time by a single-particle aerosol mass spectrometer (SPAMS, Hexin Analytical Instrument Co., Ltd., Guangzhou, China). The SPAMS system size-focuses particles via an aerodynamic lens, sizes them with two continuous 532 nm Nd:YAG lasers, and analyzes composition by laser desorption/ionization with a 266 nm pulsed laser, followed by bipolar time-of-flight mass spectrometry to obtain both positive and negative mass spectra (Li et al., 2011). Meteorological parameters (temperature and relative humidity) and

https://doi.org/10.5194/egusphere-2026-1853
Preprint. Discussion started: 5 June 2026

concentrations of regulated gases (NO_2, SO_2, and O_3) and $PM_{2.5}$ were obtained at hourly resolution from monitoring stations co-located with the SPAMS sampling sites. All online instruments underwent regular calibration and quality assurance checks throughout the campaign. Data were synchronized to Beijing time (UTC+8) and processed as hourly averages for subsequent analysis.

2.3 Single-particle data analysis

Single-particle data were processed using MATLAB with the COCO toolkit (v3.0). Across the sites, 71,392–1,347,245 particles with valid bipolar mass spectra were detected, showing a significant correlation between particle number and $PM_{2.5}$ concentrations ($r = 0.507–0.752$, $p < 0.01$; **Fig. S1**). Ba-containing particles were identified by a threshold of >5 counts on the characteristic m/z 138 peak ($[Ba^+]$), yielding 679–59,010 particles (1.0–4.4% of total). These particles were clustered using the Adaptive Resonance Theory (ART-2a) algorithm based on spectral similarity in both positive and negative ion modes (Song et al., 1999), with a vigilance factor of 0.75, a learning rate of 0.05, and 20 iterations. Particles were initially grouped into 6–17 clusters based on cationic composition (**Table 1**), whose average mass spectra are shown in **Fig. S2**. For interpretation of atmospheric processing, these clusters were then manually consolidated into four major categories based on dominant anionic signatures: OClN (rich in O^-/Cl^-/NO_3^-), N (dominant NO_3^-), NS (mixed NO_3^- and SO_4^{2-}), and S (dominant SO_4^{2-}). Notably, high-molecular-weight organic matter (HMOC) interference, characterized by dense high-mass ion clusters, was observed at the CHLK site (**Fig. S3a**). These particles were separated before classification to ensure robustness.

2.4 Episode definition

The sampling period was segmented into five phases based on pronounced fluctuations in Ba concentration. Episode boundaries were defined where hourly Ba consistently exceeded one standard deviation above the campaign mean, yielding two firework episodes and three background periods: Fireworks Episode I (FI) from February 9, 17:00 to February 18, 05:00, encompassing Chinese New Year's Eve and the Spring Festival peak; Fireworks Episode II (FII) from February 25, 00:00 to 16:00, corresponding to the Chinese Lantern Festival; and three Background periods (BI, BII, BIII) characterized by low and stable Ba concentrations. This segmentation is supported by concurrent enhancements in $PM_{2.5}$ and established firework tracers (K^+, Cl^-; **Fig. S4**) during firework episodes, establishing a robust framework for comparative analysis of fresh emissions versus aged/background aerosol conditions.

2.5 Health risk assessment

To preliminarily assess potential health risks of Ba particles, we calculated the inhalation exposure dose using the USEPA framework. The average daily exposure dose (D_{inh}) was calculated as (Kong et al., 2015):

$$D_{inh}(mgkg^{-1}day^{-1}) = \frac{C \times InhR \times EF \times ED}{BW \times AT}$$

where C is the mean hourly Ba concentration across the monitoring period. Inhalation rate (InhR) is 7.6 $m^3 \cdot day^{-1}$ for children

https://doi.org/10.5194/egusphere-2026-1853
Preprint. Discussion started: 5 June 2026

and 20 $m^3 \cdot day^{-1}$ for adults. Exposure frequency (EF) is 11 $days \cdot year^{-1}$. Exposure duration (ED) is 6 years for children and 24 years for adults. Body weight (BW) is 15 kg for children and 70 kg for adults. Averaging time (AT) for non-carcinogens is ED × 365 days.

The hazard quotient (HQ) for non-carcinogenic risk was calculated as:

$$HQ = \frac{D_{inh}}{RfD}$$

where RfD is the oral reference dose for barium (0.2 $mg \cdot kg^{-1} \cdot day^{-1}$) established by the U.S. EPA Integrated Risk Information System (IRIS, 2006). In the absence of an established inhalation reference concentration, this oral RfD is used as a conservative estimate for inhalation exposure. HQ ≤ 1 indicates low or acceptable risk, while HQ > 1 suggests potential non-carcinogenic health effects.

3 Results and discussion

3.1 Physicochemical characteristics and spatial distribution of Ba-containing particles

3.1.1 Dynamics of concentration and number of Ba

Based on comprehensive observations from four stations, fireworks were identified as the dominant aerosol source during the study period. During firework episodes, Ba concentrations increased by 17- to 40-fold, while K^+(9- to 23-fold), Cl^- (2- to 3-fold), and heavy metals such as Cu and Pb (2- to 14-fold) also rose simultaneously (**Table 2, Figs. 1 and S4**). $PM_{2.5}$ increased by 2- to 3-fold, while secondary inorganic ions (sulfate and nitrate) showed smaller increases (1- to 3-fold), indicating active atmospheric aging (Peng et al., 2021). Notably, sulfate and nitrate during FII were lower than background levels (FII/BII < 1), suggesting that this reflects the brief duration of the firework event rather than suppressed secondary formation.

The relaxation of fireworks regulations caused sharp, short-term air quality deterioration. Ba concentrations and Ba-containing particle numbers exceeded background levels by approximately two orders of magnitude, with hourly peaks up to 1000-fold. This magnitude is comparable to that of severe firework events reported globally, such as Diwali celebrations in India (Kulshrestha et al., 2004; Tanda et al., 2019; Wang et al., 2007). These enhancements are substantially greater than the 4.5- to 40-fold increases documented in regions with stricter controls, consistent with findings by Huang et al.(2024).

Diurnal variations showed concentrations rising sharply from evening, peaking at night (20:00–02:00) at levels more than an order of magnitude above background, then dropping rapidly in early morning (**Fig. 1b**). This pattern is directly linked to nighttime fireworks practices. Particle size analysis revealed significant increases in the 0.2–2.0 μm range (**Fig. 1c**). In the 0.5–1.0 μm fraction, Ba-containing particle counts surged from 2,193 during background to 24,624 during firework periods, underscoring fireworks' strong particle-generating capacity in this size range. This pronounced increase in the submicron mode is consistent with previous findings that firework-generated particles are predominantly concentrated in the

https://doi.org/10.5194/egusphere-2026-1853
Preprint. Discussion started: 5 June 2026

accumulation mode. A 6.7-fold increase in particle number concentration in the 0.5–1.0 μm range during Milan fireworks has been reported,[21] which is lower than the 11.2-fold increase observed here, suggesting particularly intense firework emissions in this study. Furthermore, more than 80% of firework-related metals, including Ba, have been found to be concentrated in the submicrometric region (<1 μm) (Crespo et al., 2012), supporting our observation that Ba-containing particles preferentially reside in the respirable size range.

3.1.2 Spatial heterogeneity across different policy zones

The observed urban–rural gradient is primarily governed by regulatory measures and human activity intensity rather than simple downwind dispersion (**Fig. 2**). The highest concentration (3,411 ng/m³) occurred at PYDXC, a restricted-fireworks suburban area with high population density (5,327 people/km²). In contrast, the urban core site (GYQ), despite higher population density (28,400 people/km²), exhibited lower peak concentrations due to a comprehensive fireworks ban. Concentrations at suburban NSPZ were slightly lower than the urban core, while rural background site (CHLK) showed the lowest levels. This pattern demonstrates that regulatory policy (ban vs. restriction) can override population density as the dominant factor governing spatial heterogeneity of peak pollution during episodic events. Combined with synchronized temporal peaks across all sites (**Fig. 1**), this provides compelling evidence that regionally synchronized emissions create a pollution field whose spatial structure is shaped by localized regulatory factors (Kong et al., 2015).

3.2 Mixing State and Identification of Fresh and Aged Particle Types

3.2.1 Mixing state and chemical characteristics of Ba-Containing particles

Fig. 3a presents the mass spectra of two representative single particles, OClN and N, which exhibit the most distinct chemical fingerprints among the four categories identified in Section 2.3. These two types were selected to illustrate the contrasting chemical features between particles with different mixing states, while the average mass spectra of the remaining types (NS and S) are provided in **Fig. S3b**. The OClN particle is characterized by intense Ba^+ [m/z 138] and BaO^+ [m/z 156] signals in the positive ion spectrum, along with prominent Cl^- [m/z –35/–37], O^- [m/z –16/–17], and NO_3^- [m/z –46/–62] peaks in the negative ion spectrum. In contrast, the N particle exhibits substantially reduced Ba^+ and BaO^+ intensities, a marked decrease in O^- and Cl^- signals, and a dominance of nitrate-related peaks [m/z –46/–62]. To quantify the distribution of these chemical types across the entire aerosol population, we examined the mixing states of all detected Ba-containing particles (**Fig. 3b**). The majority were internally mixed with nitrate (N type, 62.4%), followed by particles mixed with both chloride and nitrate (OClN type, 13.8%), and those containing sulfate (NS and S types combined, 13.6%). Particles with other mixing states accounted for the remaining 10.2%. The temporal evolution of these particle types further reveals the aging process (**Fig. 3c**). In the days preceding the Chinese New Year, OClN particles were more abundant with clear diurnal variations, while later periods saw increased proportions of aged types (N and NS). This shift provides additional evidence

https://doi.org/10.5194/egusphere-2026-1853
Preprint. Discussion started: 5 June 2026

for progressive atmospheric aging of firework-derived aerosols.

3.2.2 Evidence for fresh and aged particle types and their physical mixing

Multiple lines of evidence identify OClN particles as fresher fireworks emissions compared to N particles, which represent their more aged products. OClN particles are distinguished by enriched chloride (relative peak area of $^{35}Cl^-$ > 0.05, **Fig. S2**). Although barium chlorate [$Ba(ClO_3)_2$] is used as a green colorant, it decomposes above 250 °C and is unlikely to be emitted as such. The observed Cl^- enrichment, together with ubiquitous potassium (**Fig. 3a**), indicates OClN particles exist as chlorides (e.g., $BaCl_2$) rather than chlorate. In contrast, N particles are dominated by nitrate (**Fig. 3a**), with the combined RPA of NO_3^- and NO_2^- accounting for over 80% of the total negative ion signal (**Fig. S2**). This nitrate dominance reflects atmospheric oxidative processing, consistent with previous studies (Xue et al., 2014; Zhang et al., 2015). During the transition from firework to post-firework hours, aging was evidenced by a decrease in both the number fraction of Cl-containing particles (24% to 21%) and the relative peak area of Cl^- (0.059 to 0.040), accompanied by an increase in nitrate RPA (0.355 to 0.415) (Huang et al., 2024).

Time series analysis revealed an inverse relationship between OClN and N particles during periods of intense emissions ($r = -0.767$, $p < 0.01$; **Fig. S5a**), consistent with reported aging timescales of firework aerosols (Carrico et al., 2018; Reyes-Villegas et al., 2018). Size distributions show that N particles are preferentially found in smaller sizes compared to OClN (**Figs. S5b and S6**), consistent with increased particle density upon chloride-to-nitrate conversion during aging (Liu et al., 2017; Wang et al., 2013). Beyond chemical differences, aging also involves physical coagulation with Al- and Mg-containing particles. Al-Mg particles mixed preferentially with OClN (60–80%) over N particles (20–40%) throughout the study period (**Fig. S5c**). These single-particle observations complement bulk studies (Kong et al., 2015) by directly observing physical coagulation as an additional aging mechanism alongside chemical transformation.

3.3 Chemical transformation and aging mechanisms

3.3.1 Chemical transformation from chloride to nitrate

Synthesizing the evidence presented above, we propose that firework-derived Ba-containing particles undergo distinct aging pathways in the atmosphere. Although fresh emissions (likely $BaCl_2$) were not directly captured due to rapid atmospheric processing, OClN particles represent an early-aged state. The 9–10 hours lag between OClN and N particle peaks (Δt_1), together with the 2–4 hours lag between gaseous NO_2 and particulate NO_3^- peaks (Δt_2) (**Fig. 4a**), points to nitrate formation as a key aging pathway.

This conversion proceeds through distinct chemical stages captured by the compositional characteristics of Ba-OClN and Ba-N particles, subsets of OClN and N that are rich in Ba with minimal interference from Al and Mg, enabling direct investigation of Ba-associated chemical transformations. In Ba-OClN representing a partially aged state, peak areas of

https://doi.org/10.5194/egusphere-2026-1853
Preprint. Discussion started: 5 June 2026

chloride show a slight increase with peak areas of Ba, while nitrate signals decrease markedly (by approximately 43% from the lowest to the highest Ba interval) (**Fig. 5a**). The $Cl^-/(Cl^-+NO_3^-)$ ratio increases with Ba at lower intervals but exhibits a slight decrease at the highest Ba interval. This dominance of chloride across most Ba ranges, together with the inverse relationship between nitrate and particle mass, indicates that Ba-OClN particles are primarily composed of barium chloride ($BaCl_2$), with nitrate present as a minor component likely acquired during initial aging. The higher relative proportion of large peak areas in Ba-OClN particles (**Fig. S7**) further supports their less aged nature compared to Ba-N particles.

In contrast, Ba-N particles exhibit a distinctly different compositional pattern (**Fig. 5b**). Both chloride and nitrate peak areas increase with those of Ba, with nitrate showing a particularly strong increase at lower Ba levels followed by a clear plateau at higher Ba levels (Ba peak area > 10000). The $NO_3^-/(Cl^-+NO_3^-)$ ratio remains consistently above 0.9 across all Ba intervals. This nitrate-dominated composition, with chloride reduced to a minor residual component (<10%), indicates that Ba-N particles are primarily composed of barium nitrate [$Ba(NO_3)_2$]. The observed nitrate plateau further suggests that nitrate incorporation into Ba-containing aerosols may be self-limiting, reaching a saturation point beyond which further uptake becomes limited. This contrasts with the partially aged Ba-OClN particles, where nitrate remains a minor component and does not accumulate with increasing Ba peak area.

3.3.2 Possible aging mechanisms of Ba

Several mechanisms may contribute to the observed nitrate formation. The coexistence of O_3 and NO_2 at night is consistent with the N_2O_5 hydrolysis pathway, a common nighttime nitrate formation route (Brown et al., 2012; Zhao et al., 2023; Zhao et al., 2026). However, the moderate humidity (~60%, **Fig. S8**) during peak firework events suggests additional pathways may also be involved, such as heterogeneous uptake of HNO_3 on chlorine-rich particles (Liu et al., 2007; Vlasenko et al., 2006) or liquid-phase reactions mediated by hygroscopic salts (Cheng et al., 2016). The observed nitrate saturation in Ba-N particles likely reflects constraints on further nitrate uptake. Possible explanations include surface site limitation (Ravishankara et al., 1997), thermodynamic equilibrium with gas-phase HNO_3 (Guo et al., 2017), or phase transitions that limit internal diffusion (Koop et al., 2011). Distinguishing among these mechanisms will require further investigation using laboratory studies and thermodynamic modeling.

The aging pathways described above are further modulated by particle size, mixing state, and site-specific conditions. Notably, the nitrate fraction $[NO_3^-/(NO_3^-+Cl^-)]$ in Al-Mg-OClN particles decreases with increasing particle size, while in OClN particles without Al/Mg, this ratio shows little size dependence (**Fig. 4b**). This contrast suggests that the presence of Al and Mg may influence chloride-to-nitrate conversion efficiency (Li et al., 2023; Reinsch et al., 2010). Spatially, the extent of aging varies considerably among sites: at PYDXC, the coexistence of fresher and partially aged particles reflects active local emissions; at NSPZ, the higher abundance of aged N particles indicates more extensive aging during transport; at background sites, the dominance of fully processed, nitrate-saturated particles represent the terminal aging state under

https://doi.org/10.5194/egusphere-2026-1853
Preprint. Discussion started: 5 June 2026

regional transport influences (Zhang et al., 2019; Zhang et al., 2022). This spatial gradient provides a complementary perspective to the temporal evolution captured at individual sites, confirming that chloride-to-nitrate conversion progresses continuously during atmospheric transport (Denkenberger et al., 2007). These chemical and physical processes are not independent; chemical transformation alters particle surface properties, facilitating further coagulation, which in turn provides fresh surfaces for additional heterogeneous reactions. This interplay ultimately governs the atmospheric lifetime and transport potential of firework-derived Ba aerosols.

3.4 Health effects of Ba from fireworks

Hazard quotients (HQ) for Ba were calculated for children and adults based on measured Ba concentrations (**Table 3**). HQ values ranged from 1.22E-08 to 5.53E-06 for children and from 1.47E-08 to 3.11E-06 for adults across all sites, far below the acceptable threshold of 1, indicating negligible non-carcinogenic risks from firework-derived Ba exposure (Kulshrestha et al., 2004; Yang et al., 2015). Spatially, HQ followed the pattern of Ba concentrations, with the highest at PYDXC and the lowest at CHLK, confirming that particle concentration is the primary determinant of health risk and supporting the effectiveness of fireworks restriction policies. Children exhibited higher HQ than adults due to their greater respiratory rate per unit body weight, highlighting the need to protect sensitive populations (Kong et al., 2012; Samoli et al., 2010). Temporally, HQ during Fireworks Episode I was two orders of magnitude higher than during background periods, consistent with observations from Shanghai (Liu et al., 2019). Although the long-term risk is acceptable, this short-term peak exposure warrants attention for acute effects, particularly for individuals with respiratory conditions (Godri et al., 2012). Several uncertainties exist, including the use of oral RfD as a substitute for inhalation RfC and the lack of quantification of aging effects on Ba bioavailability (ATSDR, 2021). However, all HQ values remained substantially below 1, further demonstrating that current restriction policies effectively mitigate chronic health risks, despite transient concentration spikes during firework events.

4. Conclusions and implications

This study provides direct single-particle evidence for the aging mechanisms of firework-derived barium aerosols in urban environments. Ba concentrations increased by 1–3 orders of magnitude during firework episodes, with chlorine-rich particles (OClN) undergoing nitrate-mediated conversion to nitrate-dominated particles (N) over timescales of several hours, accompanied by physical coagulation with Al- and Mg-containing particles.

These findings have several implications. First, the rapid aging timescale (hours rather than days) suggests that secondary aerosol formation from fireworks occurs within urban airsheds, influencing local air quality prior to regional transport. Second, the observed shift toward smaller particle sizes upon chloride-to-nitrate conversion may enhance respiratory deposition potential. Third, the preferential association of Al-Mg with fresher particle populations indicates that coagulation is most active during early aging stages, potentially altering particle hygroscopicity and reactivity. Fourth, although chronic

https://doi.org/10.5194/egusphere-2026-1853
Preprint. Discussion started: 5 June 2026

health risks remain low (HQ < 1), the 1–2 order of magnitude increase in short-term exposure during firework events, particularly for children, highlights the need for targeted public health advisories. Finally, this single-particle approach offers a framework for investigating aging mechanisms of other pyrotechnic-derived metals and evaluating emission control policies beyond mass concentration metrics. Future work should examine how chloride-to-nitrate conversion influences Ba bio-availability and whether similar aging pathways apply to other metal-containing firework particles.

https://doi.org/10.5194/egusphere-2026-1853
Preprint. Discussion started: 5 June 2026

Supplement. Supporting information includes ten figures (Fig. S1-S8) related to the manuscript.

Data availability. The observational data including SPAMS and meteorological parameters used in this study are available from corresponding authors upon request (limei@jnu.edu.cn).

Author contributions. ML designed the research with input from CP, XB, GZ, and ZZ. WS, CL, LL and KH collected samples. XL processed data and wrote the manuscript. BH, and CC had an active role in supporting the writing-original work. All authors contributed to the discussions of the results and refinement of the manuscript.

Competing interests. The authors declare that they have no conflict of interest.

Financial support. This work was supported by the National Natural Science Foundation of China (grant no. 42407355).

https://doi.org/10.5194/egusphere-2026-1853
Preprint. Discussion started: 5 June 2026

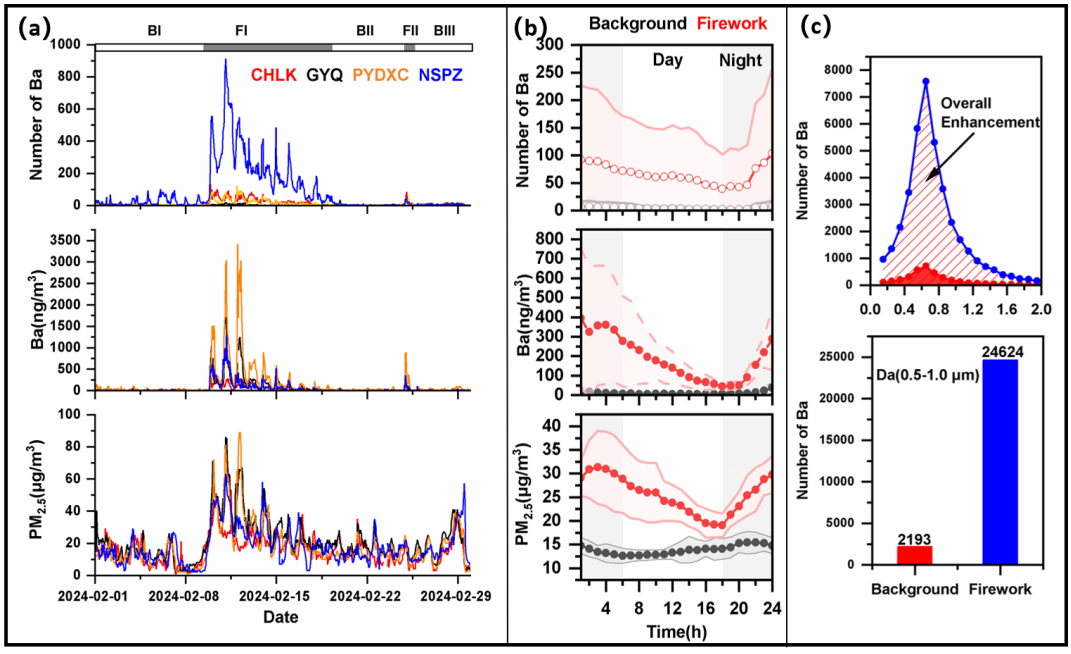

Figure 1. Temporal variations and size distributions of particulate matter. (a) Time series of $PM_{2.5}$, Ba concentration, and Ba-containing particle numbers at four sites (fireworks period shaded). (b) Diurnal patterns of $PM_{2.5}$ and Ba at the university city site during fireworks (red) and background (black). (c) Particle size distributions showing firework-induced increases of Ba-containing particles in the 0.5–1.0 μm range.

https://doi.org/10.5194/egusphere-2026-1853
Preprint. Discussion started: 5 June 2026

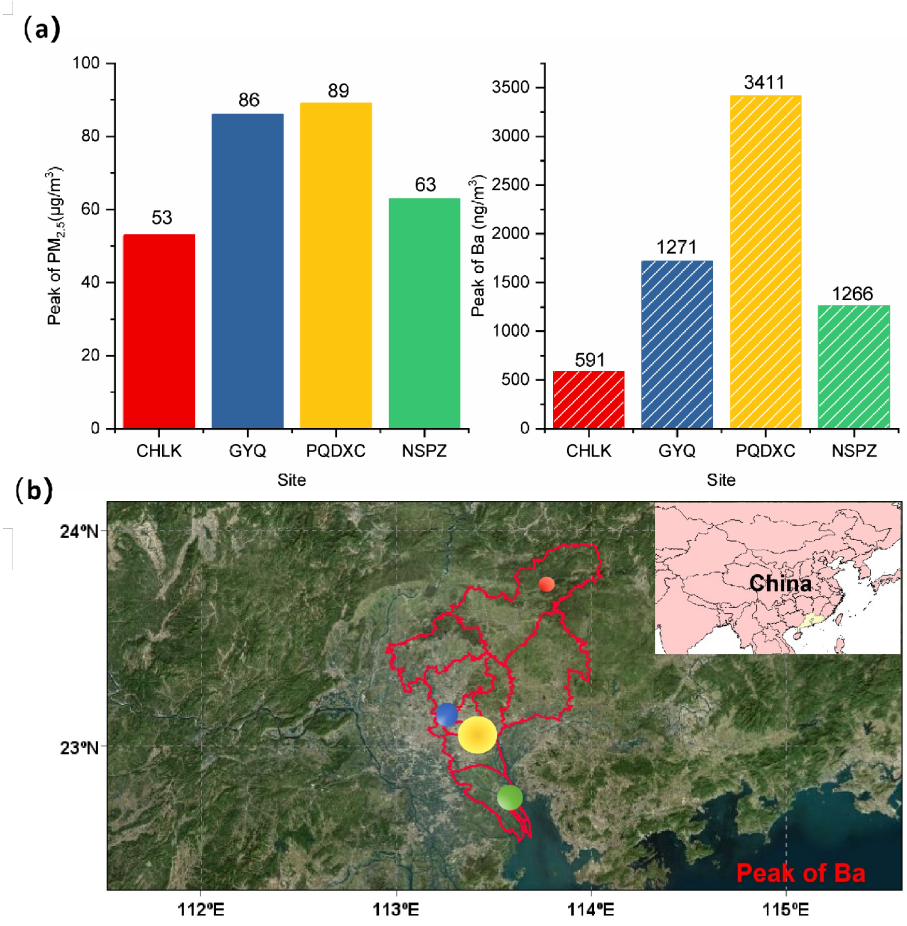

Figure 2. Spatial heterogeneity of particulate matter pollution related to fireworks. (a) Peak concentrations of $PM_{2.5}$ and peak numbers of Ba-containing particles at four monitoring points. (b) Map of the study area, where the size of the bubbles represents the specific peak $PM_{2.5}$ concentrations of each monitoring point. Basemap: Bing Satellite, processed with MeteoInfo. © Microsoft.

https://doi.org/10.5194/egusphere-2026-1853
Preprint. Discussion started: 5 June 2026

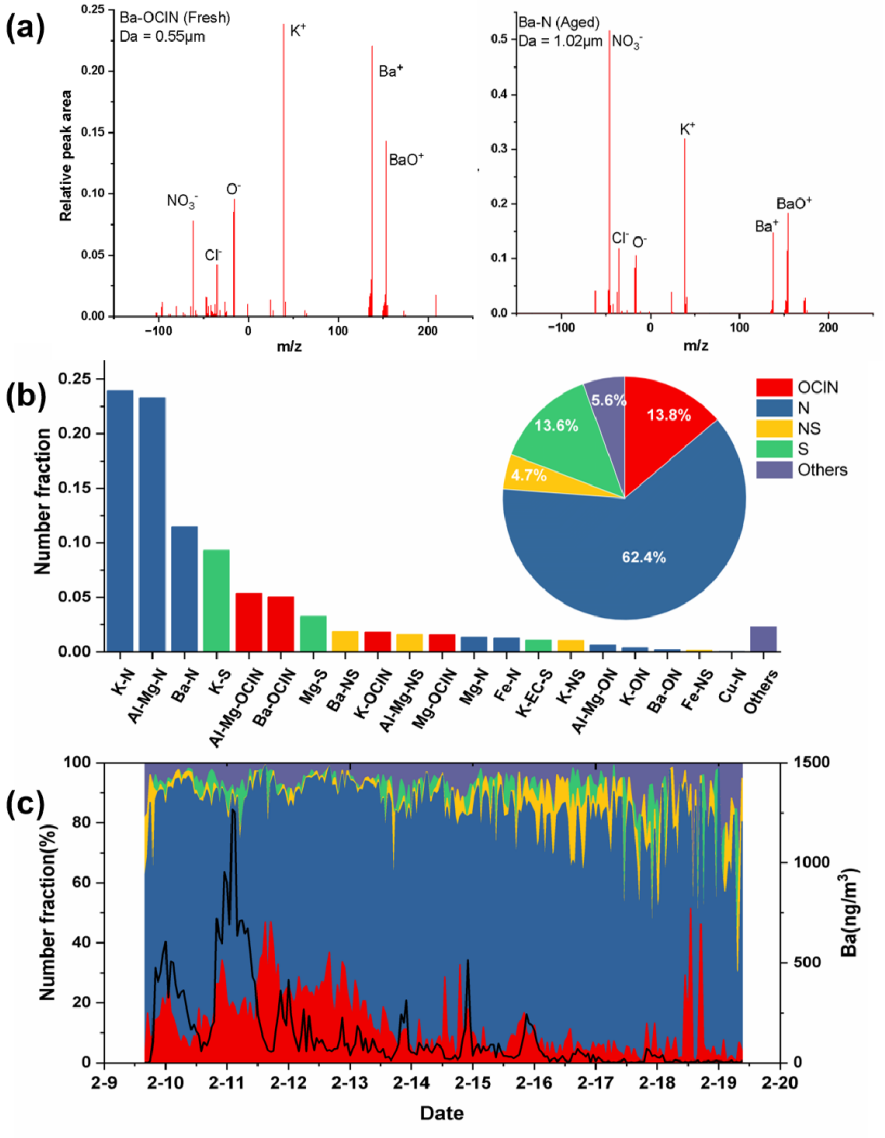

Figure 3. Chemical characteristics of Ba-containing particles during firework episodes. (a) Mass spectra of fresh (Ba-OClN) and aged (Ba-N) particle types. (b) Average abundances of particle types at four sites (bar chart) and fractional composition of reclassified groups (OClN, N, NS, S) (pie chart). (c) Temporal variations of the four main particle types (stacked bars, left axis) and Ba mass concentration (line, right axis) at four sites.

https://doi.org/10.5194/egusphere-2026-1853
Preprint. Discussion started: 5 June 2026

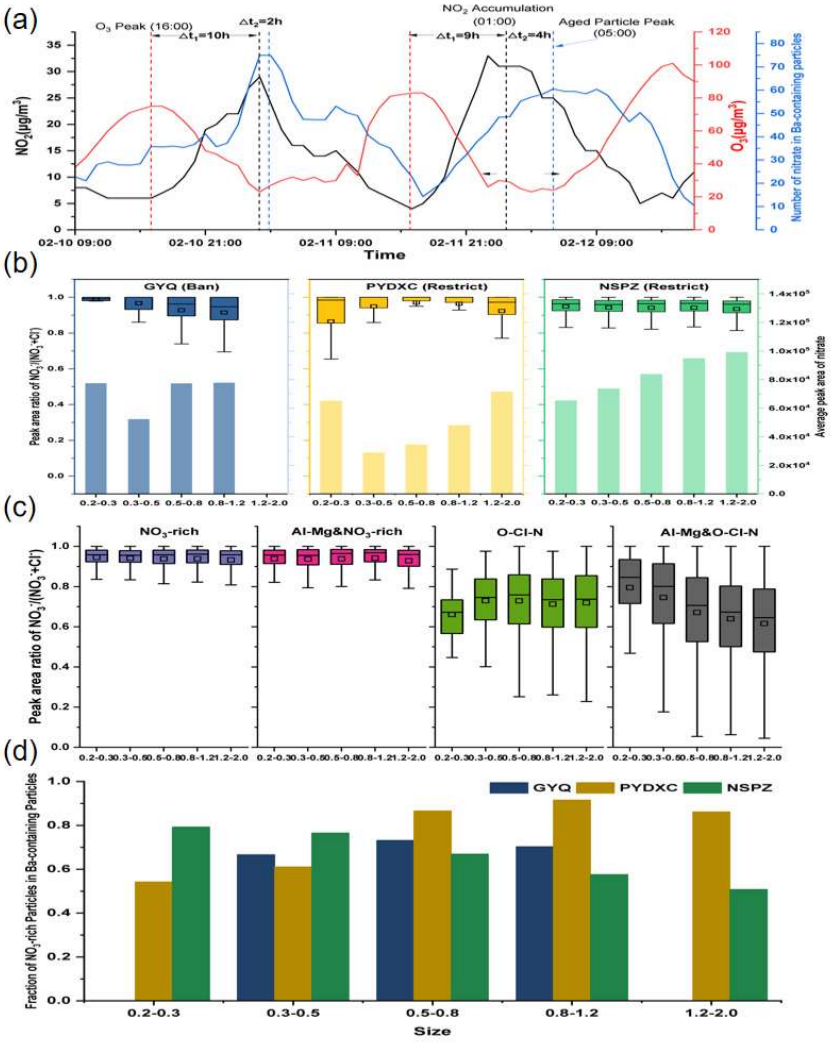

Figure 4. Nighttime aging and size-dependent nitrate formation. (a) Time series of O_3, NO_2, and nitrate-rich particles during two high-intensity firework days. (b) $NO_3^-/(NO_3^-+Cl^-)$ ratio (left) and mean nitrate peak area (right) as a function of particle size at restricted and prohibited sites. (c) $NO_3^-/(NO_3^-+Cl^-)$ ratio as a function of particle size at NSPZ during FI. (d) Fraction of nitrate-rich Ba-containing particles as a function of particle size at GYQ, PYDXC, and NSPZ.

https://doi.org/10.5194/egusphere-2026-1853
Preprint. Discussion started: 5 June 2026

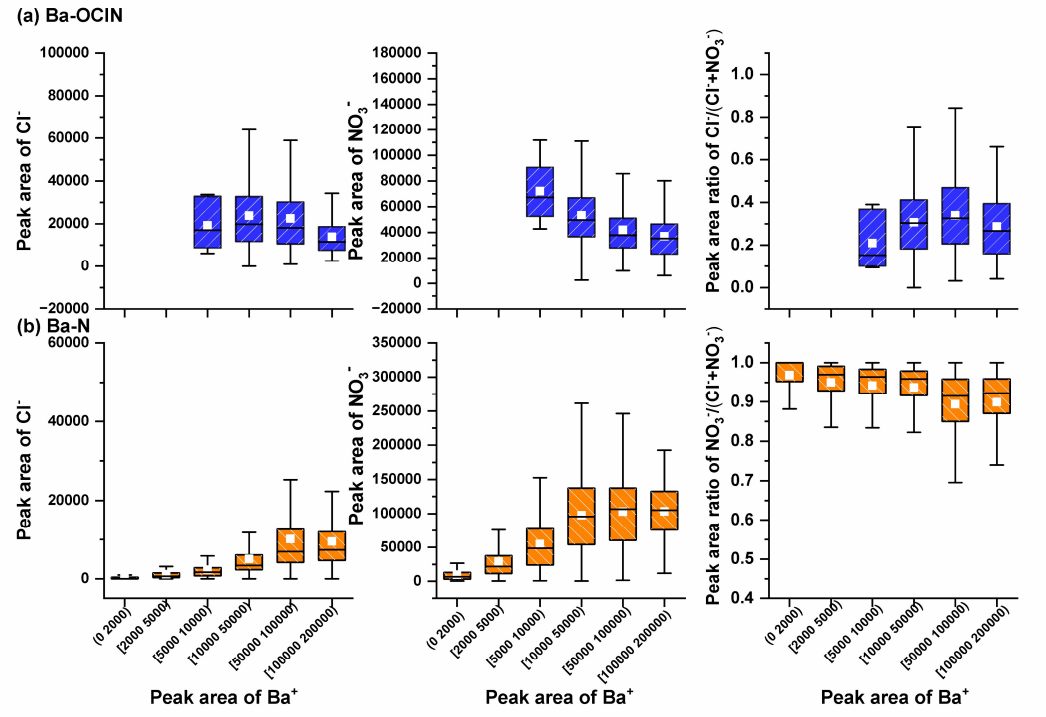

310 **Figure 5. Box plots of Cl^- peak area, NO_3^- peak area, and (a) $Cl^-/(Cl^-+NO_3^-)$ or (b) $NO_3^-/(Cl^-+NO_3^-)$ ratio as a function of Ba peak area for Ba-OClN and Ba-N particles, respectively, at the NSPZ site.**

https://doi.org/10.5194/egusphere-2026-1853
Preprint. Discussion started: 5 June 2026

Table 1 A summary of the dates of the SPAMS measurements and the number and number fraction (Nf) of the detected Ba-containing particles.

	CHLK		GYQ		PYDXC		NSPZ	
Species	Number	Nf(%)	Number	Nf(%)	Number	Nf(%)	Number	Nf(%)
All particles [a]	585933		71392		332888		1347245	
Ba-containing	8422	1.44% [b]	679	0.95%	6733	2.02%	59010	4.40%
Al-Mg-N	1396	16.6% [c]	128	18.9%	2821	41.90%	10197	17.3%
Al-Mg-OClN	802	9.5%			34	0.50%	5568	9.4%
Al-Mg-ON			33	4.9%			1727	2.9%
Al-Mg-NS	42	0.5%					407	0.7%
Ba-N	958	11.4%	111	16.3%	1345	19.98%	6732	11.4%
Ba-OClN	31	0.4%	42	6.2%			1276	2.2%
Ba-ON							518	0.9%
Ba-NS	48	0.6%					153	0.3%
K-N	2895	34.4%	247	36.4%	1601	23.78%	19713	33.4%
K-ON							901	1.5%
K-OClN	216	2.6%	79	11.6%	136	2.02%	1160	2.0%
K-NS	645	7.7%	16	2.4%			156	0.3%
K-S			11	1.6%				
K-EC-S	142	1.7%						
Mg-N	221	2.6%					1590	2.7%
Mg-OClN							3465	5.9%
Mg-S	51	0.6%						
Cu-N							112	0.2%
Fe-N	122	1.4%			364	5.41%	823	1.4%
Fe-NS	29	0.3%					108	0.2%
Others	824	9.8%	12	1.8%	432	6.42%	4404	7.5%

[a]All particles were particles with both positive and negative spectra. [b]Nf was calculated through the number of Ba-containing particles by the number of all particles over the sampling period. [c]Nf was calculated through the number of clustered Ba-containing particles by Ba-containing particles over the sampling period.

https://doi.org/10.5194/egusphere-2026-1853
Preprint. Discussion started: 5 June 2026

Table 2 The average values and standard deviations of $PM_{2.5}$, meteorological parameters, and the main water-soluble inorganic ions and heavy metals related to fireworks emissions at four stations during different pollution periods.

Parameter (Unit)	Site	BI	FI	BII	FII	BIII	FI/BI (Fold)	FII/BII (Fold)
		Mean ± SD						
$PM_{2.5}$ (μg/m³)	GYQ	11.2±6.7	21.6±8.0	13.7±5.9	7.9±5.3	14.5±9.6	1.9	0.6
	PYDXC	13.3±6.7	32.2±15.4	18.1±4.8	11.9±2.8	19.4±10.4	2.4	0.7
	NSPZ	10.0±5.6	27.7±16.9	14.0±3.9	10.4±4.7	17.5±10.3	2.8	0.7
	CHLK	11.0±6.2	25.6±12.1	14.1±5.1	12.2±4.6	18.8±10.8	2.3	0.9
Ba (ng/m³)	GYQ	2.5±2.0	84.6±91.8	4.2±17.1	25.7±60.2	2.2±1.3	33.8	6.1
	PYDXC	4.5±6.6	185.6±274.6	9.4±33.8	30.1±36.4	4.7±7.6	40.9	3.2
	NSPZ	23.0±25.2	398.5±623.5	25.1±80.0	144.1±226.4	27.0±26.3	17.3	5.8
	CHLK	4.8±6.2	137.5±207.4	8.9±35.1	42.3±53.2	7.6±11.4	28.9	4.8
K^+ (μg/m³)	GYQ	0.1±0.1	1.3±1.0	0.2±0.1	0.5±0.5	0.2±0.1	9.4	3.1
	PYDXC	0.1±0.1	1.6±2.3	0.1±0.1	0.2±0.2	0.1±0.1	23.2	1.5
	NSPZ	0.2±0.1	2.5±2.9	0.2±0.2	0.9±0.9	0.3±0.1	14.6	4.5
	CHLK	0.2±0.1	1.9±2.2	0.2±0.2	1.0±0.9	0.4±0.2	11.2	4.7
Cl^- (μg/m³)	GYQ	0.07±0.03	0.11±0.03	0.09±0.03	0.07±0.02	0.10±0.05	1.5	0.8
	PYDXC	0.3±0.3	0.7±1.2	0.2±0.1	0.2±0.1	0.4±0.4	2.6	0.9
	NSPZ	0.3±0.3	1.0±1.5	0.3±0.2	0.5±0.6	0.4±0.5	3.0	1.9
	CHLK	0.4±0.3	0.9±1.0	0.3±0.2	0.7±0.5	0.7±0.6	2.3	2.2
Cu (ng/m³)	GYQ	1.7±2.0	25.7±23.8	1.8±4.1	7.0±12.3	2.1±2.0	14.7	3.9
	PYDXC	4.3±3.2	53.8±72.2	5.0±8.6	10.2±8.2	5.9±4.7	12.5	2.0
	NSPZ	117.2±59.5	197.4±209.7	59.9±28.1	100.5±66.8	61.8±12.6	1.7	1.7
	CHLK	4.1±4.4	48.8±66.4	8.6±15.6	31.3±31.5	12.1±8.4	11.9	3.6
Pb (ng/m³)	GYQ	3.2±5.8	5.8±4.9	1.4±3.8	1.0±1.2	13.9±31.9	1.8	0.7
	PYDXC	4.1±3.5	11.6±12.1	4.8±4.6	9.3±2.8	10.3±6.0	2.8	1.9
	NSPZ	10.5±6.5	32.8±34.5	9.2±7.4	15.9±12.2	16.1±10.8	3.1	1.7
	CHLK	2.0±2.4	7.4±8.2	4.1±21.4	4.6±2.6	6.9±5.1	3.7	1.1
SO_4^{2-} (μg/m³)	GYQ	1.0±0.8	1.4±1.1	0.8±0.4	0.9±0.5	1.4±1.0	1.5	1.1
	PYDXC	3.4±2.3	4.0±1.8	2.5±0.6	2.6±0.5	3.7±2.3	1.2	1.0
	NSPZ	2.8±2.2	3.6±1.5	1.9±0.7	1.7±0.5	3.2±2.3	1.3	0.9
	CHLK	3.2±2.2	4.3±2.6	2.1±1.2	2.1±0.5	4.3±3.4	1.3	1.0
NO_3^- (μg/m³)	GYQ	1.6±1.2	4.2±1.6	4.0±3.5	1.4±1.0	2.0±1.8	2.6	0.4
	PYDXC	2.0±1.0	4.8±1.5	4.6±2.3	3.1±1.0	3.4±1.9	2.4	0.7
	NSPZ	1.9±1.0	5.1±2.2	3.8±1.8	2.3±1.6	2.7±1.7	2.7	0.6
	CHLK	1.9±0.9	5.0±2.0	4.0±2.4	3.7±0.9	3.0±1.9	2.6	0.9
SO_2 (μg/m³)	GYQ	6.4±3.5	3.2±1.1	5.2±1.7	4.4±0.7	6.6±2.6	0.5	0.9
	PYDXC	27.0±12.2	23.4±12.9	19.8±5.2	18.1±3.1	27.3±6.9	0.9	0.9
	NSPZ	24.0±14.0	13.9±7.9	17.1±6.6	13.4±3.9	26.1±10.2	0.6	0.8

https://doi.org/10.5194/egusphere-2026-1853
Preprint. Discussion started: 5 June 2026

	CHLK	28.4±16.8	17.0±9.2	23.6±11.3	16.7±4.5	30.9±12.4	0.6	0.7
	GYQ	5.7±0.6	5.6±0.7	6.1±0.5	5.3±0.6	5.6±0.7	1.0	0.9
	PYDXC	4.1±0.4	5.5±0.9	5.0±0.5	4.1±0.3	4.6±0.5	1.3	0.8
NO_2 (μg/m³)	NSPZ	5.4±1.4	8.7±1.8	4.1±1.2	5.9±0.3	6.3±0.5	1.6	1.5
	CHLK	4.3±1.0	5.1±1.1	4.8±1.0	4.2±0.4	5.4±1.1	1.2	0.9

GYQ: Gongyuanqian (urban prohibited zone); PYDXC: Panyu University City (restricted zone); NSPZ: Nansha Puzhou (restricted zone); CHLK: Conghua Liangkou (background site). The fold change (F/B) is calculated as the ratio of the average concentration during a fireworks episode to that in the preceding background period.

https://doi.org/10.5194/egusphere-2026-1853
Preprint. Discussion started: 5 June 2026

322 **Table 3 The hazard quotients (HQ) for the four stations during different pollution periods.**

Type	Site	HQ_{inh}				
		BI	FI	BII	FII	BIII
Children	CHLK	3.12E-08	1.17E-06	2.91E-08	3.56E-08	1.22E-08
	GYQ	5.62E-08	2.57E-06	6.52E-08	4.17E-08	2.60E-08
	PYDXC	2.87E-07	5.53E-06	1.74E-07	2.00E-07	1.49E-07
	NSPZ	5.99E-08	1.90E-06	6.17E-08	5.87E-08	4.21E-08
Adult	CHLK	1.76E-08	6.62E-07	1.64E-08	2.01E-08	6.88E-09
	GYQ	3.17E-08	1.45E-06	3.67E-08	2.35E-08	1.47E-08
	PYDXC	1.62E-07	3.11E-06	9.82E-08	1.12E-07	8.45E-08
	NSPZ	3.38E-08	1.07E-06	3.48E-08	3.31E-08	2.37E-08

323

https://doi.org/10.5194/egusphere-2026-1853
Preprint. Discussion started: 5 June 2026

References

Agency for Toxic Substances and Disease Registry (ATSDR).: Toxicological Profile for Barium and Barium Compounds; U.S. Department of Health and Human Services, Public Health Service: Atlanta, GA. https://www.atsdr.cdc.gov/toxprofiles/tp24.pdf, 2021.

Brown, S. S., and Stutz, J.: Nighttime Radical Observations and Chemistry. Chem. Soc. Rev. 41, 6405-6447. https://doi.org/10.1039/c2cs35181a, 2012.

Carrico, C. M., Gomez, S. L., Dubey, M. K., and Aiken, A. C.: Low Hygroscopicity of Ambient Fresh Carbonaceous Aerosols from Pyrotechnics Smoke. Atmos. Environ. 178, 101-108. https://doi.org/10.1016/j.atmosenv.2018.01.024, 2018.

Cheng, Y., Zheng, G., and Wei, C.: Reactive Nitrogen Chemistry in Aerosol Water as a Source of Sulfate during Haze Events in China. Sci. Adv. 2, e1601530. https://doi.org/10.1126/sciadv.1601530, 2016.

Conkling, J. A. and Mocella, C.: Chemistry of Pyrotechnics: Basic Principles and Theory, 2nd ed., CRC Press, Boca Raton, FL, 2010.

Crespo, J., Yubero, E., Nicolás, J. F., Lucarelli, F., Nava, S., Chiari, M., and Calzolai, G.: High-Time Resolution and Size-Segregated Elemental Composition in High-Intensity Pyrotechnic Exposures. J. Hazard. Mater. 241-242, 82-91. https://doi.org/10.1016/j.jhazmat.2012.09.017, 2012.

Deepthiraju, B., and Varma, P.: Barium Toxicity - A Rare Presentation of Fireworks Ingestion. Indian Pediatr. 49, 762-762. https://doi.org/10.1007/s13312-012-0144-z, 2012

Denkenberger, K. A., Moffet R. C., and Holecek J. C.: Real-Time, Single-Particle Measurements of Oligomers in Aged Ambient Aerosol Particles. Environ. Sci. Technol. 41, 5439-5446. https://doi.org/10.1021/es070329l, 2007.

Godri, K. J., Green, D. C., Fuller, G. W., Dall'Osto, M., Beddows, D. C., Kelly, F. J., Harrison, R., and Mudway, I.: Particulate Oxidative Burden Associated with Firework Activity. Environ. Sci. Technol. 44, 8295-8301. https://doi.org/10.1021/es1016284, 2010.

Guo, H., Liu, J., and Froyd, K. D.: Fine Particle pH and Gas-Particle Partitioning of Inorganic Species in Pasadena, California, during the 2010 CalNex Campaign. Atmos. Chem. Phys. 17, 5703-5719. https://doi.org/10.5194/acp-2016-1158, 2017.

Guangzhou Municipal People's Government. Guangzhou Fireworks and Firecrackers Safety Management Regulation. https://gzpc.gov.cn/zlk/flfgwjk/gzrdflfg/dfxfg/jk/content/post_232539.html (accessed February 11, 2026).

Hu, U., Sun, Y., Yang, G., Liu, M., Gao, Y., Lin, L., Cao, Y., Liu, W., and Huo, Y., Liu, J.: Spring Festival Firework Activities Exacerbate Toxic Effects of Aerosol Essential Components. J. Hazard. Mater. 490, 137874. https://doi.org/10.1016/j.jhazmat.2025.137874, 2025.

Huang, X., Ge, Y., Yang, T., Song, Z., Yu, S., Li, Q., Wang, X., Wang, Y., Wang, X., and Su, J.: Relaxation of Spring Festival Firework Regulations Leads to a Deterioration in Air Quality. Environ. Sci. Technol. 58, 10185-10194. https://doi.org/10.1021/acs.est.4c00920, 2024.

Inomata, Y., Igarashi, Y., Chiba, M., Shinoda, Y., and Takahashi, H.: Dry and Wet Deposition of Water-Insoluble Dust and Water-Soluble Chemical Species during Spring 2007 in Tsukuba, Japan. Atmos. Environ. 43, 4503-4512. https://doi.org/10.1016/j.atmosenv.2009.06.048, 2009.

Kaur, A., and Parkash, C.: Barium: Presence in Environment and Health Effects. Ecol. Environ. Conserv. 28, 2210-2213. https://doi.org/10.53550/eec.2022.v28i04.085, 2022.

Kong, S., Lu, B., Ji, Y., Zhao, X., Bai, Z., Xu, Y., Liu, Y., and Jiang, H.: Risk Assessment of Heavy Metals in Road and Soil Dusts within $PM_{2.5}$, PM_{10} and PM100 Fractions in Dongying City, Shandong Province, China. J. Environ. Monit. 14,

https://doi.org/10.5194/egusphere-2026-1853
Preprint. Discussion started: 5 June 2026

791-803. https://doi.org/10.1039/C1EM10555H, 2012.

Kong, S. F., Li, L., Li, X. X., Yin, Y., Chen, K., Liu, D. T., Yuan, L., Zhang, Y. J., Shan, Y. P., and Ji, Y. Q. The Impacts of Firework Burning at the Chinese Spring Festival on Air Quality: Insights of Tracers, Source Evolution and Aging Processes. Atmos. Chem. Phys. 15, 2167-2184. https://doi.org/10.5194/acp-15-2167-2015, 2015.

Koop, T., Bookhold, J., and Shiraiwa, M.: Glass Transition and Phase State of Organic Compounds: Dependency on Molecular Properties and Implications for Secondary Organic Aerosols in the Atmosphere. Phys. Chem. Chem. Phys. 13, 19238-19255. https://doi.org/10.1039/c1cp22617g, 2011.

Kulshrestha, U. C., Nageswara Rao, T., Azhaguvel, S., and Kulshrestha, M.: Emissions and Accumulation of Metals in the Atmosphere Due to Crackers and Sparkles during Diwali Festival in India. Atmos. Environ.38, 4421-4425. https://doi.org/10.1016/j.atmosenv.2004.05.044, 2004.

Lee, E. S., Sahay, K., O'Neil, E., Biswas, S., Dzhema, I., Huang, S.-M., Lin, P., Chang, M.-C. O., and Huai, T.: Tracer-Gas-Integrated Measurements of Brake-Wear Particulate Matter Emissions from Heavy-Duty Vehicles. Environ. Sci. Technol. 57, 15968-15978. https://doi.org/10.1021/acs.est.3c03673, 2023.

Li, W., Shi, Z., Yan, C., Yang, L., Dong, C., and Wang, W.: Individual Metal-Bearing Particles in a Regional Haze Caused by Firecracker and Firework Emissions. Sci. Total Environ. 443, 464-469. https://doi.org/10.1016/j.scitotenv.2012.10.109, 2013.

Li, L., Huang, Z., Dong, J., Li, M., Gao, W., Nian, H., Fu, Z., Zhang, G., Bi, X., and Cheng, P.: Real Time Bipolar Time-of-Flight Mass Spectrometer for Analyzing Single Aerosol Particles. Int. J. Mass Spectrom. 303, 118-124. https://doi.org/j.ijms.2011.01.017, 2011.

Li, Y., Zhou, Y., and Guo, W.: Molecular Imaging Reveals Two Distinct Mixing States of $PM_{2.5}$ Particles Sampled in a Typical Beijing Winter Pollution Case. Environ. Sci. Technol. 57, 10236-10245. https://doi.org/10.1021/acs.est.2c08694, 2023.

Liu, D., Whitehead, J., Alfarra, M. R., Reyes-Villegas, E., Spracklen, D. V., Reddington, C. L., Kong, S., Williams, P. I., and Ting, Y. C., and Haslett, S.: Black-Carbon Absorption Enhancement in the Atmosphere Determined by Particle Mixing State. Nat. Geosci.10, 184-188, https://doi.org/10.1038/ngeo2901, 2017.

Liu, J., Chen, Y., Chao, S., Cao, H., Zhang, A., 2019. Levels and Health Risks of $PM_{2.5}$-Bound Toxic Metals from Firework/Firecracker Burning during Festival Periods in Response to Management Strategies. Ecotoxicol. Environ. Saf. 171, 406-413. https://doi.org/10.1016/j.ecoenv.2018.12.104, 2019.

Liu, Y., Cain, J. P., Wang, H., and Laskin, A.: Kinetic Study of Heterogeneous Reaction of Deliquesced NaCl Particles with Gaseous HNO_3 Using Particle-on-Substrate Stagnation Flow Reactor Approach. Environ. Sci. Technol. 41, 6497-6502. https://doi.org/10.1021/jp072005p, 2007.

Peng, J., Hu, M., Shang, D., Wu, Z., Du, Z., Tan, T., Wang, Y., Zhang, F., and Zhang, R.: Explosive Secondary Aerosol Formation during Severe Haze in the North China Plain. Environ. Sci. Technol. 55, 2189-2207. https://doi.org/10.1021/acs.est.0c07204, 2021.

Ravishankara, A. R.: Heterogeneous and Multiphase Chemistry in the Troposphere. Science 1997, 276, 1058-1065. https://doi.org/10.1126/science.276.5315.1058, 1997.

Reinsch, B. C., Forsberg, B. , and Penn, R. L.: Chemical Transformations during Aging of Zerovalent Iron Nanoparticles in the Presence of Common Groundwater Dissolved Constituents. Environ. Sci. Technol. 44, 3455-3461. https://doi.org/10.1021/es902924h, 2010.

Reyes-Villegas, E., Priestley, M., Ting, Y. C., Haslett, S., Bannan, T., Le Breton, M., Williams, P. I., Bacak, A., Flynn, M. J., and Coe, H.: Simultaneous Aerosol Mass Spectrometry and Chemical Ionisation Mass Spectrometry Measurements during a Biomass Burning Event in the UK: Insights into Nitrate Chemistry. Atmos. Chem. Phys. 18, 4093-4111. https://doi.org/10.5194/acp-2017-60510.5194, 2018.

https://doi.org/10.5194/egusphere-2026-1853
Preprint. Discussion started: 5 June 2026

Salma, I., Farkas, Á., and Weidinger, T.: Balogh, M. Firework Smoke: Impacts on Urban Air Quality and Deposition in the Human Respiratory System. Environ. Pollut. 328, 121612. https://doi.org/10.1016/j.envpol. 2023.121612, 2023.

Samoli, E., Nastos, P., Paliatsos, A., Katsouyanni, K., and Priftis, K.: Acute Effects of Air Pollution on Paediatric Asthma Exacerbation: Evidence of Association and Effect Modification. Eur. Respir. J. 36 (Suppl. 54), 523s. https://doi.org/10.7490/F1000RESEARCH.523.1, 2010.

Sharma, R., and Thakur, S.: Chapter 36-Barium Sulfate: Human Effects Assessment and Toxicological Profile. In Hazardous Chemicals, Chawla, M., Singh, J., Kaushik, R. D., Eds., Academic Press, pp 517-531, 2025.

Song, X. H., Hopke, P. K., Fergenson, D. P., and Prather, K. A.: Classification of Single Particles Analyzed by ATOFMS Using an Artificial Neural Network, ART-2A. Anal. Chem. 71, 860-865. https://doi.org/10.1021/ac9809682, 1999.

Tanda, S., Libinsk, R., Hegrová, J., and Goessler, W.: Impact of New Year's Eve Fireworks on the Size Resolved Element Distributions in Airborne Particles. Environ. Int. 128, 371-378. https://doi.org/10.1016/j.envint.2019.04.071, 2019.

Twohy, C., and Doran, C.: Field Performance Evaluation of the Cooper Environmental Services Ambient Metals Monitor (Xact 620) for Near-Real Time PM_{10} Metals Monitoring, Cooper Environmental Services. http://aaarabstracts.com/2010/viewabstract.php?id=788, 2010.

Vecchi, R., Bernardoni, V., Cricchio, D., D'Alessandro, A., Fermo, P., Lucarelli, F., Nava, S., Piazzalunga, A., and Valli, G.: The Impact of Fireworks on Airborne Particles. Atmos. Environ. 42, 1121-1132. https://doi.org/10.1016/j.atmosenv.2007.10.047, 2008.

Vlasenko, A., Sjogren, S., and Weingartner, E.: Effect of Humidity on Nitric Acid Uptake to Mineral Dust Aerosol Particles. Atmos. Chem. Phys. 6, 2147-2160. https://doi.org/10.5194/acp-6-2147-2006, 2006.

Wang, G. H., Zhou, B. H., Cheng, C. L., Cao, J. J., Li, J. J., Meng, J. J., Tao, J., Zhang, R. J., and Fu, P. Q.: Impact of Gobi Desert Dust on Aerosol Chemistry of Xi'an, Inland China during Spring 2009: Differences in Composition and Size Distribution between the Urban Ground Surface and the Mountain Atmosphere. Atmos. Chem. Phys. 13, 819-835. https://doi.org/10.5194/acp-13-819-2013, 2013.

Wang, W., Zhou, H., Gao, Y., Shao, L., Zhou, X., Li, X., Wei, D., Xing, J., and Lyu, R.: Chemical Composition and Morphology of $PM_{2.5}$ in a Rural Valley during Chinese New Year's Eve: Impact of Firework/Firecracker Display. Atmos. Environ. 318, 120225. https://doi.org/10.1016/j.atmosres.2016.07.028, 2024.

Wang, Y., Zhuang, G., Xu, C., and An, Z.: The Air Pollution Caused by the Burning of Fireworks during the Lantern Festival in Beijing. Atmos. Environ. 41, 417-431. https://doi.org/10.1016/j.atmosenv.2006.07.043, 2007.

Webster, H., Visible Spectra of Standard Navy Colored Flares. Propellants, Explos., Pyrotech. 10, 1-4. https://doi.org/10.1002/prep.19850100102, 1985.

Xue, J., Yuan, Z., Lau, A. K. H., and Yu, J. Z.:Insights into Factors Affecting Nitrate in $PM_{2.5}$ in a Polluted High NOx Environment through Hourly Observations and Size Distribution Measurements. J. Geophys. Res.: Atmos. 119, 4888-4902. https://doi.org/10.1002/2013JD021108, 2014.

Yang, Z., Liu, Y., Wang, X., Zhong, Z., Zhu, M., and Zhang, L.: Influence of Fireworks Igniting in Spring Festival of 2014 on Heavy Metal Content of Beijing Dust. Meteorol. Environ. Res. 6, 14-21, https://doi.org/CNKI:SUN:MEVR.0.2015-Z2-003, 2015.

Zhang, H., Guo, H., Hu, J., Ying, Q., and Kleeman, M. J.: Modeling Atmospheric Age Distribution of Elemental Carbon Using a Regional Age-Resolved Particle Representation Framework. Environ. Sci. Technol. 53, 270-278. https://doi.org/10.1021/acs.est.8b05895, 2019.

Zhang, R., Wang, G., Guo, S., Zamora, M. L., and Wang, Y.: Formation of Urban Fine Particulate Matter. Chem. Rev. 115, 3803-3855. https://doi.org/10.1021/acs.chemrev.5b00067, 2015.

Zhang, H., Worton, D. R., Shen, S., Nah, T., Isaacman-VanWertz, G., Wilson, K. R., and Goldstein, A. H.: Fundamental Time Scales Governing Organic Aerosol Multiphase Partitioning and Oxidative Aging, Environ. Sci. Technol., 49, 9768–9777,

https://doi.org/10.5194/egusphere-2026-1853
Preprint. Discussion started: 5 June 2026

https://doi.org/10.1021/acs.est.5b02115, 2015.

Zhao, X., Zhao, X., Liu, P. Chen, D., Zhang, C., Xue, C., Liu, J., and Mu. Y.: Transport Pathways of Nitrate Formed from Nocturnal N_2O_5 Hydrolysis Aloft to the Ground Level in Winter North China Plain. Environ. Sci. Technol. 57, 5108-5118. https://doi.org/10.1021/acs.est.4c02495, 2023.

Zhao, X., Zhao, X., Zhu, W., Liu, Z., and Hu, B.: Formation Dominated by Nocturnal N_2O_5 Hydrolysis in Urban Areas Driven by Regional Atmospheric Transport. Environ. Sci. Technol. 60. https://doi.org/10.1021/acs.est.6c02100, 2026.

Zhong, H., Huang, R.-J., and Lin, C.: Measurement Report: On the Contribution of Long-Distance Transport to the Secondary Aerosol Formation and Aging. Atmos. Chem. Phys. 22, 9513-9524. https://doi.org/10.5194/acp-2022-270, 2022.